Thermodynamics of silicate liquids in the deep Earth

Lars Stixrude [a],*, Nico de Koker [b], Ni Sun [b], Mainak Mookherjee [c], Bijaya B. Karki [d,e]

[a] Department of Earth Sciences, University College London, Gower Street, London, WC1E 6BT, United Kingdom
[b] Department of Geological Sciences, University of Michigan, Ann Arbor, MI 48109-1005, United States
[c] Bayerisches Geoinstitut, University of Bayreuth, D-95444 Bayreuth, Germany
[d] Department of Computer Science, Louisiana State University, Baton Rouge, LA 70803, United States
[e] Department of Geology and Geophysics, Louisiana State University, Baton Rouge, LA 70803, United States

ABSTRACT

We discuss the geophysical implications of recent first principles molecular dynamics simulations of $MgSiO_3$ liquid, in particular the findings that the Grüneisen parameter increases by a factor of three on two-fold compression, and the predicted melting curve. The predicted melting temperature of $MgSiO_3$ perovskite at 136 GPa is 5400±600 K, which if lowered by freezing point depression by 1300 K, yields a mantle solidus temperature of 4100 K, identical to recent estimates of the temperature at the base of the mantle. We argue on this basis that partial melting at the base of the mantle is plausible. While $MgSiO_3$ perovskite is denser than the isochemical liquid, reasonable values of iron partitioning and bulk iron contents, leads to the conclusion that a melt at the base of the multi-component mantle would be denser than its surroundings and therefore buoyantly stable. We predict the bulk sound velocity of this melt to be 10.9 km s^{-1}, less than that of ultra-low velocity zones, and consistent with the explanation of these regions as being due to partial melting. The increase on compression of the Grüneisen parameter in the liquid state yields isentropes that are much hotter than previously thought: a potential temperature of only 2450 K is sufficient to melt the entire mantle, and a magma ocean will begin crystallization at mid-mantle depths, rather than at the base of the mantle.

© 2008 Elsevier B.V. All rights reserved.

1. Introduction

Silicate liquids are primary agents of the thermal and chemical evolution of Earth. Evidence that they have played an important role in Earth's evolution at depths substantially greater than that of present day magma genesis include that of the giant moon-forming impact early in Earth's history (Canup, 2004), which may have left the mantle largely or completely molten, xenoliths that have been brought to the surface from 400 km or even substantially deeper (Haggerty and Sautter, 1990), komatiitic lavas that may have been produced by partial melting in upwellings beginning at shallow lower mantle conditions (Herzberg, 1995), and the presence of ultra-low velocity zones at the base of the mantle that have been interpreted as partial melts (Williams and Garnero, 1996).

Despite their importance to understanding Earth's history, little is known of silicate liquids at pressures beyond those of the upper mantle. Published pre-heated shock wave experiments have to date achieved pressures of 40 GPa, less than one third that of the mantle's base (Rigden et al., 1989). Shock experiments from ambient initial conditions, which produce liquid via dynamic compression, have reached substantially higher pressures (Akins et al., 2004; Mosenfelder et al., 2007), but are more challenging to interpret because several solid–solid phase transitions occur along the Hugoniot in addition to melting and because melting

appears to be over-driven. Other means of constraining the thermodynamics of silicate liquids are so far restricted to lower pressures including measurements of the density and sound speed near ambient conditions (Lange, 1997), and sink-float experiments (Sakamaki et al., 2006).

In order to understand the thermodynamics of silicate liquids in this little-explored realm, we have used first principles molecular dynamics simulations. These calculations make no assumption as to the nature of bonding or the shape of the charge density and are thus in principle equally applicable to all elements of the periodic table and all pressure–temperature conditions. Moreover, there are no free parameters in the theory, which lends it predictive power.

In this study, we explore the geophysical implications of our simulations on $MgSiO_3$ liquid (Stixrude and Karki, 2005), including: 1) the Grüneisen parameter, which we have found behaves very differently from previous expectations with important implications for the thermal state of a deep magma ocean, 2) the density contrast between liquids and co-existing solids in the deep mantle and the possibility of neutrally buoyant melt at the base of the mantle, 3) the seismological signature of a partial melt at the base of the mantle.

2. Theory

We emphasize an improved thermodynamic analysis of the results of our first principles molecular dynamics simulations (de Koker et al.,

* Corresponding author.
  E-mail address: l.stixrude@ucl.ac.uk (L. Stixrude).

2008), which has the advantage of being self-consistent, and which permits a more extensive exploration of geophysically relevant thermodynamic properties. The computational details of the molecular dyamics simulations themselves can be found in our previous publications and are reviewed here briefly (Stixrude and Karki, 2005).

Our first principles molecular dynamics simulations are based on density functional theory in the Local Density Approximation (LDA), using the plane-wave pseudopotential method as implemented in the VASP code (Kresse and Furthmuller, 1996). Born–Oppenheimer simulations were performed in the canonical ensemble with a Nosé (1984) thermostat with 80 atoms, and run for at least 3000 steps at 1 fs time step. We assume thermal equilibrium between ions and electrons via the Mermin functional (Mermin, 1965). Tests using larger systems, up to 336 atoms, and greater run durations, up to 8000 time steps, showed no significant change in equilibrium thermodynamic properties. The Brillouin zone is sampled at zero-wavector ($k=0$, Γ point). The basis-set size is set by the value of the energy cutoff of 400 eV.

At each time step, we compute the internal energy, stress tensor and forces acting on the nuclei, which drive the Newtonian dynamics. The thermodynamic average values of the internal energy and pressure are determined from the time average, via the ergodic hypothesis, after discarding the first 20% of time steps to allow for transients. Uncertainties are computed using the appropriate non-Gaussian statistics via the blocking method (Flyvbjerg and Petersen, 1989). Two corrections of order a few GPa are made to the pressure: the Pulay correction to account for the finite basis set, and an empirical correction to account for the small but systematic error in the local density approximation. Further details of our simulation methods are given in other publications (de Koker et al., 2008; Karki et al., 1997).

Thermodynamic properties computed from our simulations are adequately described by the fundamental thermodynamic relation (Callen, 1960; de Koker et al., 2008)

$$F(V,T) = F_0 + F_C(V,T_0) + F_{TH}(V,T) \tag{1}$$

where the "cold" part of the Helmholtz free energy F_C is that of Birch–Murnaghan Eulerian finite strain theory

$$F_C = 9K_0 V_0 \left(\frac{1}{2}f^2 + \frac{1}{6}a_3 f^3 + ... \right) \tag{2}$$

with

$$f = \frac{1}{2}\left| \left(\frac{V}{V_0}\right)^{-2/3} - 1 \right| \tag{3}$$

$$\partial_3 = 3\left(K_0' - 4\right) \tag{4}$$

and the thermal part

$$F_{TH}(V,T) = -(F_0 - E_0)\left(\frac{T}{T_0} - 1\right) - C_V\left[T\ln\frac{T}{T_0} - (T-T_0)\right]$$
$$- C_V(T-T_0)\left[(\gamma_0 - \gamma')\ln\frac{V}{V_0} + \gamma - \gamma_0\right] \tag{5}$$

where subscript 0 indicates values at the reference volume V_0 and temperature T_0, K is the isothermal bulk modulus, K' is isothermal pressure derivative, E is the internal energy, and C_V is the isochoric heat capacity.

We find that the Grüneisen parameter is adequately represented by

$$\gamma(V) = \gamma_0 + \gamma'\left(\frac{V}{V_0} - 1\right) \tag{6}$$

The value of γ and C_V are computed from our simulations form the isochoric variation of E and P with T, according the identities:

$\gamma = V(\partial P/\partial E)_V$ and $C_V = (\partial E/\partial T)_V$. To within the resolution of our simulations, γ and C_V are independent of temperature. The Maxwell relation

$$\frac{1}{T}\left(\frac{\partial C_V}{\partial V}\right)_T = \frac{1}{V}\left(\frac{\partial(\gamma C_V)}{\partial T}\right)_V \tag{7}$$

then demands that C_V be independent of volume. In fact, we find from our simulations a weak volume dependence to C_V (10% decrease over two-fold compression), implying also a slight temperature dependence to C_V and γ, which however is sufficiently small that Eqs. (1)–(6) with constant C_V describes simulated values of pressure and internal energy to within uncertainty. The value of C_V for silicate liquids deviates substantially from the Dulong–Petit value (de Koker et al., 2008; Mookherjee et al., 2008; Stixrude and Karki, 2005): e.g. $C_V = 3.7R$ at 30 GPa in $MgSiO_3$ liquid, where R is the gas constant.

The pressure, internal energy, enthalpy, and isothermal and adiabatic bulk moduli are derived from the fundamental relation via derivatives and Legendre transformations as

$$P(V,T) = -\left(\frac{\partial F}{\partial V}\right)_T = 3K_0 f(2f+1)^{5/2}\left(1 + \frac{a_3}{2}f + \frac{a_4}{6}f^2 + ...\right) + \frac{\gamma}{V}C_V(T-T_0) \tag{8}$$

$$E(V,T) = F - T\left(\frac{\partial F}{\partial T}\right)_V = E_0 + F_C + C_V(T-T_0) + C_V\left[(\gamma_0 - \gamma')\ln\frac{V}{V_0} + \gamma - \gamma_0\right] \tag{9}$$

$$H(P,T) = E(V,T) + P(V,T)V \tag{10}$$

$$K = V\left(\frac{\partial^2 F}{\partial V^2}\right) \tag{11}$$

$$K_S = K + \gamma^2 C_V T/V \tag{12}$$

where K_S is the adiabatic bulk modulus. From the bulk modulus, we may compute the P-wave velocity of the liquid

$$v_P = \sqrt{\frac{K_S + 4/3\mu}{\rho}} = \sqrt{\frac{K_S}{\rho}} \tag{13}$$

where ρ is the mass density, μ is the shear modulus, and the last equality follows if the frequency of the seismic probe is much smaller than the characteristic frequency of shear relaxation in the liquid, in which case $\mu \to 0$, as found experimentally (Rivers and Carmichael, 1987).

We compute adiabatic temperature profiles of $MgSiO_3$ liquid and perovskite by integrating

$$\left(\frac{\partial T}{\partial P}\right)_S = \frac{\gamma T}{K_S} \tag{14}$$

from an assumed surface potential temperature T_0 and using our simulated values of γ and K_S.

We determine the melting curve via the Clapeyron equation

$$\left(\frac{\partial T_M}{\partial P}\right)_{eq} = \left(\frac{\Delta V}{\Delta H/T_M}\right) \tag{15}$$

where T_M is the melting temperature, and ΔV and ΔH are, respectively the volume and enthalpy difference between solid and liquid. The quantities ΔV and ΔH are determined directly from our simulations. The integration constant is set by assuming one fixed point along the melting curve. We choose this point as 25 GPa and 2900 K near the low pressure limit of perovskite melting where many experiments are mutually consistent (Ito and Katsura, 1992; Shen and Lazor, 1995; Sweeney and Heinz, 1998; Zerr and Boehler, 1993).

3. Results

The melting curve of $MgSiO_3$ perovskite increases monotonically with increasing pressure over the range of our simulations, reaching a temperature of 5400±600 K at the core–mantle boundary (Stixrude and Karki, 2005) (Fig. 1). The positive melting slope reflects the greater density of perovskite as compared with the isochemical liquid over the entire pressure–temperature range of our study. The mantle solidus is estimated to lie 800–1300 K below that of $MgSiO_3$ perovskite (Zhou and Miller, 1997). We have estimated the mantle solidus based on our melting curve of $MgSiO_3$ perovskite assuming that freezing point depression varies linearly with pressure from the experimentally determined value of 340 K at 25 GPa (Tronnes and Frost, 2002), to a value at the upper end of the range of previous estimates (1300 K) at the base of the mantle. This yields a solidus temperature of 4100 K at the base of the mantle, consistent with an experimental constraint based on shock compression of natural olivines that the solidus temperature be less than 4300±270 K (Holland and Ahrens, 1997), and with extrapolations of measurements to 60 GPa of the peridotite and basalt solidi (Hirose et al., 1999; Zerr et al., 1998). Our estimate of the solidus temperature at the base of the mantle is identical to recent estimates of the temperature at the core–mantle boundary based on the equation of state of liquid iron, and the elasticity of the inner core (Steinle-Neumann et al., 2002), and the core solidus (Nimmo et al., 2004). A more secure estimate of freezing point depression at the bottom of the mantle awaits determinations of the melting lines of other important mantle components including MgO [currently highly uncertain (Zerr and Boehler, 1994; Zhang and Fei, 2008)] as well as determinations of the free energy of solution in the liquid state at
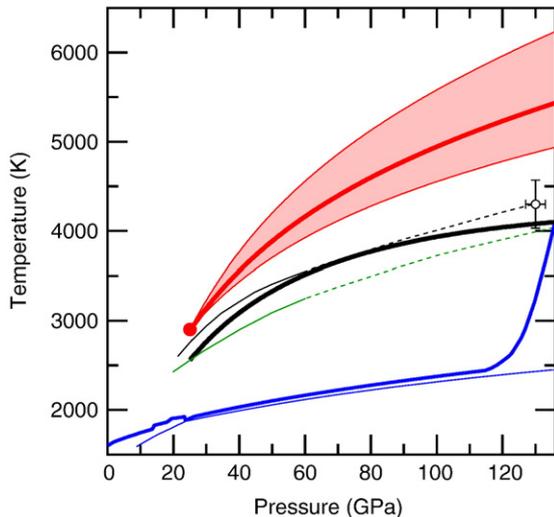

Fig. 2. Volume (top, blue solid line) and entropy (bottom, red solid line) of fusion of $MgSiO_3$ perovskite from first principles molecular dynamics simulations compared with experimental values at 1 bar (Lange, 1997; Stebbins et al., 1984) (symbols) and pressure-independent theoretical results for idealized one-component systems with repulsive forces proportional to r^{-n} with $n=1$ (one-component plasma, ocp), 6, 12, and $n{\to}\infty$ (hard spheres).

Fig. 1. Predicted melting curve of $MgSiO_3$ perovskite (red line with shaded uncertainty envelope) compared with a modern mantle geotherm (blue thick line) represented by the $T_0=1600$ K isentrope (Stixrude and Lithgow-Bertelloni, 2007) and a lower thermal boundary layer that reaches a temperature of 4100 K at the core–mantle boundary (Nimmo et al., 2004; Steinle−Neumann et al., 2002). The form of the thermal boundary layer shown is consistent with models based on observed seismic discontinuities in D″ and the location of the perovskite to post-perovskite phase boundary (Lay et al., 2006). For comparison (blue thin line), we also show the geotherm of Brown and Shankland (1981). The mantle solidus $T_{sol}(P)$ (bold black solid line) is estimated as $T_{sol}(P)=T_{pv}(P)-T_{fp}(P)$ where T_{pv} is the melting curve of $MgSiO_3$ perovskite from our simulations, and T_{fp} is the freezing point depression which is assumed to vary linearly with pressure from the experimental value at 25 GPa (340 K) (Tronnes and Frost, 2002) to 1300 K at 136 GPa (Zhou and Miller, 1997). For comparison we show previous experimentally-based estimates of the mantle solidus including upper bounds on the peridotite solidus (symbol: (Holland and Ahrens, 1997); thin black line: (Zerr et al., 1998)), and the basalt solidus (thin green line: (Hirose et al., 1999)). The thin lines are drawn as solid over the range of measurements, and dashed in extrapolation.
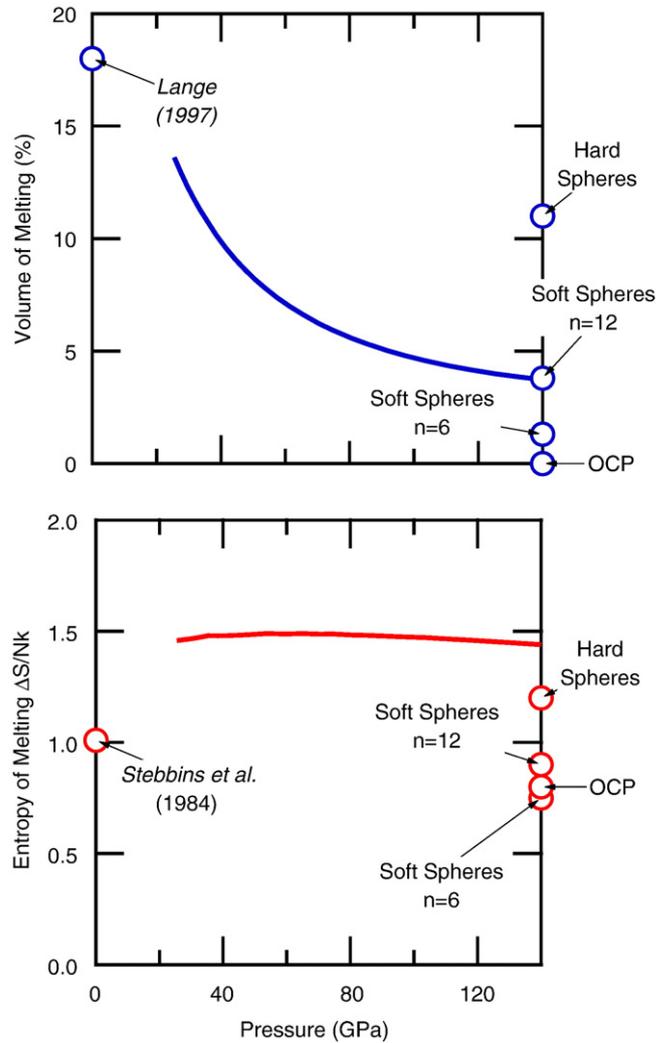
lower mantle pressure (currently unknown from either experiment or first principles theory).

Although the volume of melting is always positive, it decreases in magnitude rapidly with increasing pressure (Stixrude and Karki, 2005) (Fig. 2). While at low pressure, the volume of melting is large (18%) (Lange and Carmichael, 1987), at the core–mantle boundary it is reduced by a factor of nearly 5 to 4%. The high pressure volume of melting falls within the range expected for simple systems, including monatomic liquids with atoms interacting via inverse power law repulsion with power n, which have universal values of the volume of melting ranging from 4% for $n=12$ to 0% for the one-component plasma ($n=1$). Despite this similarity, it is likely that the volume of melting of $MgSiO_3$ composition will continue to decrease with increasing pressure, and may even become negative at pressures beyond those at the base of the mantle (Akins et al., 2004).

The entropy of melting varies slowly with compression and is substantially larger than that of simple close-packed liquids (Stixrude and Karki, 2005) (Fig. 2). Whereas the entropy of melting of $MgSiO_3$ perovskite is 1.5 Nk, that of inverse power law fluids fall in the range 0.7–0.9 Nk, as it does for many monatomic materials at high pressure (Stishov et al., 1973). The reason for this difference is that the silicate
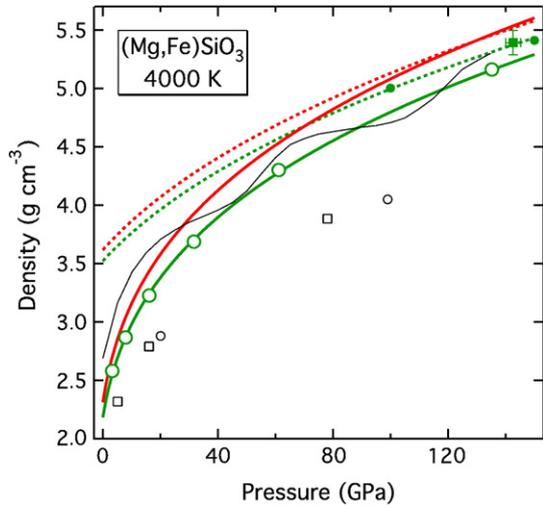
Fig. 3. Density of liquid (solid lines) and perovskite (dashed lines) of MgSiO₃ composition (green) and with added iron as described in the text (red) at 4000 K based on our FPMD results compared with our FPMD results for MgSiO₃ liquid (open green circles) and MgSiO₃ perovskite (solid green circles) at 4000 K, the experimental measurement of perovskite by Luo et al. (2004) at 4130 K (green square with error bars, P. D. Asimow, personal communication), the results of non-first principles rigid ion molecular dynamics simulations of MgSiO₃ liquid by Wasserman et al. (1993) at 4500 K (open black squares) and Zhou and Miller (Zhou and Miller, 1997) at 5000 K (open black circles), and a speciation model calculation at 1673 K (Ghiorso, 2004) (thin black line).

The rapid decrease in the volume of melting suggests that the liquid–solid density contrast at high pressure is dominated by compositional differences between liquid and coexisting solids, rather than the volume contrast itself (Stixrude and Karki, 2005). To evaluate the possible influence of heavy major element partitioning on the liquid–solid density contrast, we compute the density of iron-bearing MgSiO₃ liquid and perovskite assuming 1) the perovskite–liquid iron partition coefficient $K_{Fe}=Fe_{Pv}Mg_L/(Fe_LMg_{Pv})=0.4$ consistent with experiments at lower pressure (Ito and Takahashi, 1987; Knittle, 1998; McFarlane et al., 1994; Tronnes and Frost, 2002), 2) that the influence of iron substitution on the density is similar in liquid and solid, and 3) the bulk iron content of the mantle $X_{Fe}=Fe/(Mg+Fe)=0.1$. We find that the liquid is denser than the solid at 4000 K and pressures greater than 130 GPa (Fig. 3). A subsequent FPMD study of MgSiO₃ liquid also found that a deep melt may be denser than its surroundings (Wan et al., 2007).

We find that the bulk sound velocity of MgSiO₃ and Mg₂SiO₄ liquids at 136 GPa and 4000 K are remarkably similar to each other and approximately 20% less than that of the P-wave velocity of the global seismic model PREM (Fig. 4). The bulk sound velocity of the liquid is likely to be further reduced by partitioning of heavy major elements. Accounting for preferential partitioning of iron into the liquid as above, the velocity contrast is increased to 23%.

The Grüneisen parameter of MgSiO₃ liquid increases by a factor of three on two-fold compression (Stixrude and Karki, 2005). This behavior is opposite to that of all mantle crystalline phases (Stixrude and Lithgow-Bertelloni, 2005), and to previous assumptions regarding

liquid has many more degrees of freedom than the simple liquids, whose structures are close-packed. The configurational entropy of the silicate liquid is greater and this accounts for the greater entropy of melting. The high pressure entropy of melting is greater than that at zero pressure ($\Delta S=1.0 Nk$). This is likely due to the greater variety of coordination environments in the liquid at high pressure. Whereas at low pressure, the liquid has dominantly 4-fold Si–O coordination, at high pressure a greater variety of Si–O coordination environments are present ranging from 4-fold to 7-fold at 100 GPa.
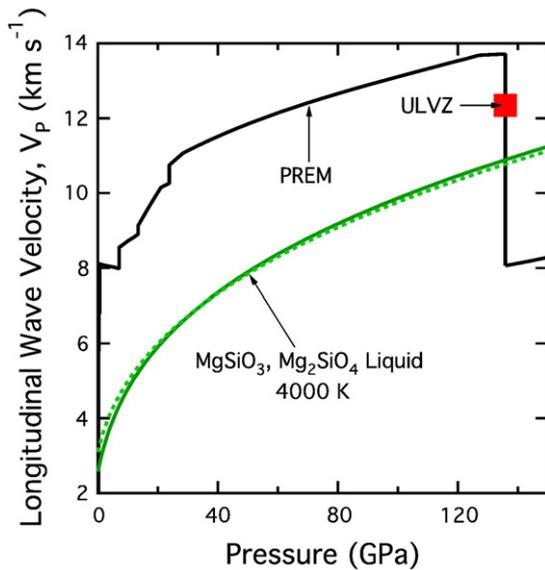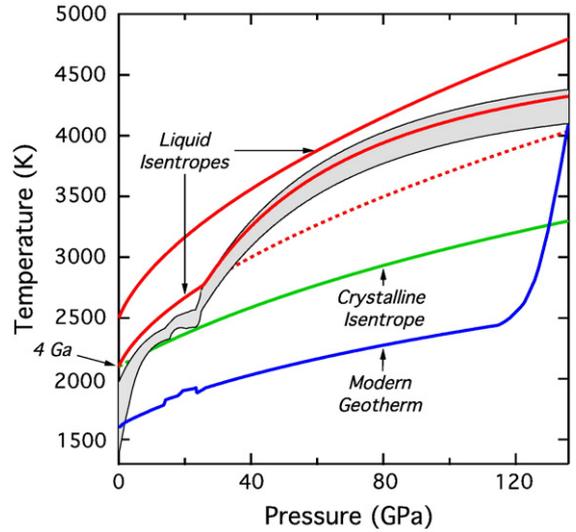

Fig. 4. The longitudinal wave velocity of MgSiO₃ (green solid line), and Mg₂SiO₄ (green dashed line) liquid at 4000 K from our FPMD simulations compared with that of the global seismic model PREM (Dziewonski and Anderson, 1981) (black) and a representative value for ultra-low velocity zones (red square) (Williams and Garnero, 1996).

Fig. 5. Isentropes of MgSiO₃ liquid (red) with $T_0=2100$ K and $T_0=2500$ K, and MgSiO₃ perovskite (green) with $T_0=2100$ K, drawn within the stability field (solid) and as metastable continuations outside the stability field (short dashed) compared with a modern mantle geotherm (blue, as described in Fig. 1). The grey envelope represents the mantle melting interval constrained by experiment up to 25 GPa (Ito et al., 2004; Tronnes and Frost, 2002; Zhang and Herzberg, 1994), and at higher pressure by our predicted melting curve of MgSiO₃ perovskite (Stixrude and Karki, 2005) and freezing point depression as described in Fig. 1. The liquidus temperature in the lower mantle is estimated by assuming that the ratio of liquidus (T_L) to solidus (T_S) temperature remains fixed at the experimentally constrained value at 25 GPa throughout the lower mantle $T_L/T_S=1.07$, consistent with the cryoscopic equation, and our finding from first principles molecular dynamics simulations that the entropy of melting of MgSiO₃ perovksite remains nearly constant through the lower mantle. In detail, the ratio T_L/T_S may change with increasing pressure with changes in the eutectic liquid composition. The bold red line representing the $T_0=2100$ K isentrope accounts for the effects of partial melting ("wet" adiabat) and lies between solidus and liquidus at pressure greater than 26 GPa. The influence of partial melting on the isentrope is modeled by assuming that the entropy varies linearly within the melting interval: $S(T)=S_{pv}(T)+[S_l(T)-S_{pv}(T)](T-T_{sol})/(T_{liq}-T_{sol})$, where S_{pv} and S_l are the entropy of MgSiO₃ perovskite and liquid, respectively, and T_{sol} and T_{liq} are the solidus and liquidus temperatures, respectively.

the volume dependence of γ in silicate liquids (Miller et al., 1991a; Rigden et al., 1989; Stixrude and Bukowinski, 1990). The Grüneisen parameter had previously been found to increase on compression in non-silicate liquids (Boehler and Ramakrishnan, 1980; Knopoff and Shapiro, 1970; Vocadlo et al., 2003). Very recently our prediction that this behavior should occur in silicate liquids has been confirmed experimentally (Mosenfelder et al., 2007). The unusual behavior of the Grüneisen parameter can be rationalized in terms of pressure-induced structural changes (Stixrude and Karki, 2005).

The increase of γ on compression has a large influence on the adiabatic temperature profile of a putative magma ocean via Eq. (14) which shows that the adiabatic gradient is directly proportional to γ (Fig. 5). We find that for a potential temperature $T_0 = 2100$ K, thought to be representative of the Archean mantle (Herzberg, 1995), the liquid adiabat is superliquidus from the surface to 26 GPa, and its metastable continuation reaches 4000 K at the base of the mantle. We also compare with a crystalline adiabat with $T_0 = 2100$ K, which is metastable at shallow depths. At the base of the mantle, the liquid adiabat is 800 K higher than a crystalline adiabat of the same potential temperature. The temperature contrast across the mantle along the liquid adiabat (1900 K) is more than twice that along the present day crystalline mantle adiabat (900 K). Potential temperatures as low as $T_0 = 2450$ K produce complete melting of the mantle, representing a magma ocean extending to the core–mantle boundary. The temperature at the base of a completely molten mantle for $T_0 = 2500$ K is 4800 K. The nearest approach of the mantle to the liquidus, occurs at mid-mantle depths.

Taking into account the influence of partial melting ("wet" adiabat), the $T_0 = 2100$ K isentrope lies between solidus and liquidus from 26 GPa to the base of the mantle. The wet adiabat has the unusual property that the melt fraction increases with increasing pressure for pressure greater than 70 GPa. This is caused by the large dT/dP slope of the liquid-state isentropes as compared with the dT/dP slope of the liquidus and solidus.

4. Discussion

Previous studies of silicate liquids had assumed that the Grüneisen parameter decreased with compression according to the relation

$$\gamma = \gamma_0 \left(\frac{V}{V_0} \right)^q \tag{16}$$

with $q = 1$, in which case the ratio γ/V is a constant (Miller et al., 1991a; Rigden et al., 1989; Stixrude and Bukowinski, 1990). This approximation was motivated, at least in part, by the behavior of mantle crystalline phases, which show values of q that in many cases are indistinguishable from unity, and that in all cases are positive (Stixrude and Lithgow-Bertelloni, 2005). In contrast, we find that γ increases with decreasing volume, so that q must be negative. As our results demand that q vary with compression, they are better represented by the linear form (Eq. (6)) than by Eq. (16). For purposes of illustration, we may compute a mean value of q over the entire compression range of our study as $\overline{q} = \frac{\Delta \ln \gamma}{\Delta \ln V} = -1.6$, where the Δ symbol represents the difference between our largest and smallest volume results. Subsequently, we have found that γ increases on compression in other compositions as well, so that this is likely a universal feature of silicate liquids (de Koker et al., 2008; Karki et al., 2007; Mookherjee et al., 2008).

The influence of the Grüneisen parameter on the isentrope can be understood via

$$\left(\frac{\partial S}{\partial \ln V} \right)_T = \gamma C_V \tag{17}$$

which shows that entropy decreases on compression. Since C_V changes little on compression, the rate at which S decreases is

governed by the value and volume dependence of γ. As we find that γ takes on much higher values at high pressure than previously suspected, the entropy of the liquid decreases much more rapidly on compression than previously thought. Since our results show that the entropy at high pressure is everywhere less than previously assumed, the isentropic temperature must be correspondingly greater. This, along with the greater compressibility of the liquid, accounts for the much greater temperature increase with compression along the liquid, as compared with the solid isentrope.

Our finding that the Grüneisen parameter of the liquid increases on compression has important implications for the Hadean mantle. Complete melting of the mantle occurs at much lower potential temperatures than previously thought: the mantle is superliquidus for $T_0 \geq 2450$ K, (Fig. 5). In contrast, Miller et al. (1991b), assuming $q = 1$, find that the mantle is completely superliquidus for potential temperatures $T_0 \geq 3500$ K, while Abe (1997) find that for a potential temperature $T_0 = 3000$ K, the mantle is superliquidus only to a pressure of 40 GPa. Whereas we find the $T_0 = 2500$ K isentrope to be super-liquidus throughout the mantle, the $T_0 = 2500$ K liquid isentrope of Miller et al. (1991b) intersects the liquidus at 45 GPa and 3000 K, whereas that of Abe (1997) intersects the liquidus at 18 GPa and 2800 K. Instead we find that the $T_0 = 2500$ K liquid isentrope lies at a temperature of 3100 K at 18 GPa, and 3640 K at 45 GPa.

In our analysis, the mantle melts at lower potential temperature because the temperature contrast across a molten mantle, and therefore the temperature at its base is much higher than previously thought for a given potential temperature. Whereas we find a temperature contrast across the mantle of 1900 K along the 2500 K adiabat, Miller et al. (1991b) find a temperature contrast of only 1300 K for a much hotter adiabat (3500 K), the coldest in their analysis that produces a super-liquidus mantle. Similar results have been obtained by (Mosenfelder et al., 2007) who also emphasized the role of γ increasing on compression. The value of γ at high compression deduced from their experiments is even larger than what we find from simulations of forsterite liquid, although experiment and simulation agree on the values of the directly measured quantities (density, pressure, energy) to within uncertainty (de Koker et al., 2008).

Crystallization of an initially molten mantle begins at mid-mantle depths, rather than at the base of the mantle as found in many previous analyses that did not take into account the increase of γ with compression (Miller et al., 1991b; Solomatov, 2000; Walter and Tronnes, 2004). In the shallow Earth, magma genesis occurs primarily by decompression melting because the adiabatic gradient is much less than the slope of the solidus. Most previous studies of the Hadean mantle have assumed that the solidus remains steeper than the adiabat throughout most of the mantle. The consequence of this assumption is that crystallization of a magma ocean begins at its base. However, we have found that the adiabatic gradient is much steeper at high pressure than previously thought, and may exceed the slope of the solidus in the lower mantle. We find that the liquid isentrope will first intersect the liquidus at 70 GPa and 3900 K (Fig. 5).

The deep mantle may be partially molten today. Our results indicate that melt may be thermodynamically and buoyantly stable at the base of the mantle (Figs. 1 and 3). The physical properties of a partial melt at the base of the mantle are consistent with those determined by seismological studies of ultra-low velocity zones (Fig. 4). The density of liquid and solid phases predicted by our FPMD simulations differs by large amounts from that of previous predictions based on semi-empirical rigid ion interaction potentials (Wasserman et al., 1993; Zhou and Miller, 1997), and speciation models (Ghiorso, 2004) (Fig. 4). These comparisons highlight the importance of the more accurate first principles approach, which makes no a priori assumptions regarding structure, bonding, or the shape of the charge density.

Our conclusions regarding the thermodynamic stability of melt at the base of the present mantle and the depth of initial crystallization

of a magma ocean are necessarily limited by our current ignorance of freezing point depression in the deep mantle. This uncertainty emphasizes the need for experimental and theoretical investigations of the phase equilibria of multi-component compositions at lower mantle pressures. For example, it has recently been found that the solubility of water in silicate melt is likely to be unlimited over nearly the entire mantle pressure range (Mookherjee et al., 2008). If even a small fraction of the water budget of chondrite-like precursors were delivered to the deep Earth, this may have produced a hydrous magma ocean with a considerably lower solidus than the values we have considered in our analysis.

5. Conclusions

Silicate liquids are fundamentally different from their crystalline counterparts in that their structure changes continuously on compression. This structural change has important implications for thermodynamic properties, including the Grüneisen parameter, and for our understanding of the early Earth and melt at depth in the present mantle.

Our analysis indicates that less energy than previously thought need be delivered to the accreting Earth to melt it entirely. Since the increase of temperature with depth along the isentrope is the result of gravitational self-compression, the amount of energy required to melt the mantle is measured by the potential temperature. Models of Earth's accretion and early evolution should re-investigate the possibility that energy delivered by impacts, core formation, or short-lived radio-isotopes may be sufficient entirely to melt the mantle. Such a scenario, in which the Earth is completely molten, contrasts with models of early Earth in which the magma ocean occupies the outer part of the mantle and is underlain by a largely unmelted silicate layer (Li and Agee, 1996; Ohtani, 1985; Wood et al., 2006).

Models of magma ocean evolution should account for the possibility that crystallization begins in the mid-mantle, and that the crystallizing layer will separate two liquid regions: one extending to the surface, and another extending to the core–mantle boundary, with potentially distinct thermal and chemical evolutionary histories. The existence of a basal liquid layer may have important implications for the generation and preservation of ancient mantle geochemical signatures, and for the origin of ultra-low velocity zones and large scale thermochemical anomalies in the lower mantle (Boyet and Carlson, 2005; Labrosse et al., 2007).

Acknowledgments

References

Abe, Y., 1997. Thermal and chemical evolution of the terrestrial magma ocean. Phys. Earth Planet. Inter. 100 (1–4), 27–39.

Akins, J.A., Luo, S.N., Asimow, P.D., Ahrens, T.J., 2004. Shock-induced melting of MgSiO3 perovskite and implications for melts in Earth's lowermost mantle. Geophys. Res. Lett. 31 (14).

Boehler, R., Ramakrishnan, J., 1980. Experimental results on the pressure-dependence of the Gruneisen-parameter—a review. J. Geophys. Res. 85 (NB12), 6996–7002.

Boyet, M., Carlson, R.W., 2005. Nd-142 evidence for early (>4.53 Ga) global differentiation of the silicate Earth. Science 309 (5734), 576–581.

Brown, J.M., Shankland, T.J., 1981. Thermodynamic parameters in the earth as determined from seismic profiles. Geophys. J. R. Astron. Soc. 66 (3), 579–596.

Callen, H.B., 1960. Thermodynamics. John Wiley and Sons, New York. 376 pp.

Canup, R.M., 2004. Simulations of a late lunar-forming impact. Icarus 168 (2), 433–456.

de Koker, N.P., Stixrude, L., Karki, B.B., 2008. Thermodynamics, structure, dynamics, and freezing of Mg2SiO4 liquid at high pressure. Geochim. Cosmochim. Acta 72 (5), 1427–1441.

Dziewonski, A.M., Anderson, D.L., 1981. Preliminary reference earth model. Phys. Earth Planet. Inter. 25, 297–356.

Flyvbjerg, H., Petersen, H.G., 1989. Error-estimates on averages of correlated data. J. Chem. Phys. 91 (1), 461–466.

Ghiorso, M.S., 2004. An equation of state for silicate melts. III. Analysis of stoichiometric liquids at elevated pressure: shock compression data, molecular dynamics simulations and mineral fusion curves. Am. J. Sci. 304 (8–9), 752–810.

Haggerty, S.E., Sautter, V., 1990. Ultradeep (greater than 300 kilometers), ultramafic upper mantle xenoliths. Science 248 (4958), 993–996.

Herzberg, C., 1995. Generation of plume magmas through time—an experimental perspective. Chem. Geol. 126 (1), 1–16.

Hirose, K., Fei, Y.W., Ma, Y.Z., Mao, H.K., 1999. The fate of subducted basaltic crust in the Earth's lower mantle. Nature 397 (6714), 53–56.

Holland, K.G., Ahrens, T.J., 1997. Melting of (Mg,Fe)2SiO4 at the core–mantle boundary of the Earth. Science 275, 1623–1625.

Ito, E., Katsura, T., 1992. Melting of ferromagnesian silicates under the lower mantle conditions. In: Syono, Y., Manghnani, M.H. (Eds.), High-pressure Research: Application to Earth and Planetary Sciences. American Geophysical Union, Washington, DC, pp. 315–322.

Ito, E., Takahashi, E., 1987. Melting of peridotite at uppermost lower-mantle conditions. Nature 328 (6130), 514–517.

Ito, E., Kubo, A., Katsura, T., Walter, M.J., 2004. Melting experiments of mantle materials under lower mantle conditions with implications for magma ocean differentiation. Phys. Earth Planet. Inter. 143–44, 397–406.

Karki, B.B., et al., 1997. Structure and elasticity of MgO at high pressure. Am. Mineral. 82, 51–60.

Karki, B.B., Bhattarai, D., Stixrude, L., 2007. First-principles simulations of liquid silica: structural and dynamical behavior at high pressure. Phys. Rev., B 76 (10).

Knittle, E., 1998. The solid/liquid partitioning of major and radiogenic elements at lower mantle pressures: implications for the core–mantle boundary region, core–mantle boundary region. Geodyn. Ser. 119–130.

Knopoff, L., Shapiro, J.N., 1970. Pseudo–Grüneisen parameter for liquids. Phys. Rev., B 1 (10), 3893–3895.

Kresse, G., Furthmuller, J., 1996. Efficient iterative schemes for ab initio total-energy calculations using a plane-wave basis set. Phys. Rev., B 54 (16), 11169–11186.

Labrosse, S., Hernlund, J.W., Coltice, N., 2007. A crystallizing dense magma ocean at the base of the Earth's mantle. Nature 450 (7171), 866–869.

Lange, R.A., 1997. A revised model for the density and thermal expansivity of K2O-Na2O-CaO-MgO-Al2O3-SiO2 liquids from 700 to 1900 K: extension to crustal magmatic temperatures. Contrib. Mineral. Petrol. 130 (1), 1–11.

Lange, R.A., Carmichael, I.S.E., 1987. Densities of Na2o-K2o-Cao-Mgo-Feo-Fe2o3-Al2o3-Tio2-Sio2 liquids—new measurements and derived partial molar properties. Geochim. Cosmochim. Acta 51 (11), 2931–2946.

Lay, T., Hernlund, J., Garnero, E.J., Thorne, M.S., 2006. A post-perovskite lens and D″ heat flux beneath the central Pacific. Science 314 (5803), 1272–1276.

Li, J., Agee, C.B., 1996. Geochemistry of mantle–core differentiation at high pressure. Nature 381 (6584), 686–689.

Luo, S.N., Akins, J.A., Ahrens, T.J., Asimow, P.D., 2004. Shock-compressed MgSiO3 glass, enstatite, olivine, and quartz: optical emission, temperatures, and melting. J. Geophys. Res.-Solid Earth 109 (B5).

McFarlane, E.A., Drake, M.J., Rubie, D.C., 1994. Element partitioning between Mg–perovskite, magnesiowustite, and silicate melt at conditions of the earths mantle. Geochim. Cosmochim. Acta 58 (23), 5161–5172.

Mermin, N.D., 1965. Thermal properties of inhomogeneous electron gas. Phys. Rev. 137 (5A), A1441–A1443.

Miller, G.H., Stolper, E.M., Ahrens, T.J., 1991a. The equation of state of a molten komatiite.1. Shock-wave compression to 36 Gpa. J. Geophys. Res.-Solid Earth and Planets 96 (B7), 11831–11848.

Miller, G.H., Stolper, E.M., Ahrens, T.J., 1991b. The equation of state of a molten komatiite.2. Application to komatiite petrogenesis and the Hadean mantle. J. Geophys. Res.-Solid Earth and Planets 96 (B7), 11849–11864.

Mookherjee, M., Stixrude, L., Karki, B., 2008. Hydrous silicate melt at high pressure. Nature 452 (7190), 983–986.

Mosenfelder, J.L., Asimow, P.D., Ahrens, T.J., 2007. Thermodynamic properties of Mg2SiO4 liquid at ultra-high pressures from shock measurements to 200 GPa on forsterite and wadsleyite. J. Geophys. Res.-Solid Earth 112 (B6).

Nimmo, F., Price, G.D., Brodholt, J., Gubbins, D., 2004. The influence of potassium on core and geodynamo evolution. Geophys. J. Int. 156 (2), 363–376.

Nosé, S., 1984. A molecular-dynamics method for simulations in the canonical ensemble. Mol. Phys. 52, 255–268.

Ohtani, E., 1985. The primordial terrestrial magma ocean and its implication for stratification of the mantle. Phys. Earth Planet. Inter. 38 (1), 70–80.

Rigden, S.M., Ahrens, T.J., Stolper, E.M., 1989. High-pressure equation of state of molten anorthite and diopside. J. Geophys. Res. 94, 9508–9522.

Rivers, M.L., Carmichael, I.S.E., 1987. Ultrasonic studies of silicate melts. J. Geophys. Res.-Solid Earth And Planets 92 (B9), 9247–9270.

Sakamaki, T., Suzuki, A., Ohtani, E., 2006. Stability of hydrous melt at the base of the Earth's upper mantle. Nature 439 (7073), 192–194.

Shen, G.Y., Lazor, P., 1995. Measurement of melting temperatures of some minerals under lower mantle pressures. J. Geophys. Res.-Solid Earth 100 (B9), 17699–17713.

Solomatov, V.S., 2000. Fluid dynamics of a terrestrial magma ocean. In: Canup, R.M. (Ed.), Origin of the Earth Moon. University of Arizona Press, Tucson, pp. 323–338.

Stebbins, J.F., Carmichael, I.S.E., Moret, L.K., 1984. Heat-capacities and entropies of silicate liquids and glasses. Contrib. Mineral. Petrol. 86 (2), 131–148.

Steinle-Neumann, G., Stixrude, L., Cohen, R.E., 2002. Physical properties of iron in the inner core. In: Dehant, V., Creager, K., Zatman, S., Karato, S.-I. (Eds.), Core Structure, Dynamics, and Rotation. American Geophysical Union, Washington, DC, pp. 137–161.

Stishov, S.M., Makarenk, In, Ivanov, V.A., Nikolaen, Am, 1973. Entropy of melting. Phys. Lett., A 45 (1), 18-18 A.

Stixrude, L, Bukowinski, M.S.T., 1990. Fundamental thermodynamic relations and silicate melting with implications for the constitution of D". J. Geophys. Res. 95, 19311–19325.

Stixrude, L., Karki, B., 2005. Structure and freezing of MgSiO$_3$ liquid in Earth's lower mantle. Science 310 (5746), 297–299.

Stixrude, L., Lithgow-Bertelloni, C., 2005. Thermodynamics of mantle minerals—I. Physical properties. Geophys. J. Int. 162 (2), 610–632.

Stixrude, L., Lithgow-Bertelloni, C., 2007. Influence of phase transformations on lateral heterogeneity and dynamics in Earth's mantle. Earth Planet. Sci. Lett. 263, 45–55, doi:10.1016/j.epsl.2007.08.027.

Sweeney, J.S., Heinz, D.L., 1998. Laser-heating through a diamond-anvil cell: melting at high pressures. In: Manghnani, M.H., Yagi, T. (Eds.), Properties of Earth and Planetary Materials at High Pressure and Temperature. American Geophysical Union, Washington, D. C., pp. 197–213.

Tronnes, R.G., Frost, D.J., 2002. Peridotite melting and mineral-melt partitioning of major and minor elements at 22–24.5 GPa. Earth Planet. Sci. Lett. 197 (1–2), 117–131.

Vocadlo, L., Alfe, D., Gillan, M.J., Price, G.D., 2003. The properties of iron under core conditions from first principles calculations. Phys. Earth Planet. Inter. 140 (1–3), 101–125.

Walter, M.J., Tronnes, R.G., 2004. Early Earth differentiation. Earth Planet. Sci. Lett. 225 (3–4), 253–269.

Wan, J.T.K., Duffy, T.S., Scandolo, S., Car, R., 2007. First-principles study of density, viscosity, and diffusion coefficients of liquid MgSiO3 at conditions of the Earth's deep mantle. J. Geophys. Res.-Solid Earth 112 (B3).

Wasserman, E.A., Yuen, D.A., Rustad, J.R., 1993. Molecular-dynamics study of the transport-properties of perovskite melts under high-temperature and pressure conditions. Earth Planet. Sci. Lett. 114 (2–3), 373–384.

Williams, Q., Garnero, E.J., 1996. Seismic evidence for partial melt at the base of earth's mantle. Science 273, 1528.

Wood, B.J., Walter, M.J., Wade, J., 2006. Accretion of the Earth and segregation of its core. Nature 441 (7095), 825–833.

Zerr, A., Boehler, R., 1993. Melting of (Mg,Fe)SiO3 perovskite to 625 kilobars: indication of a high melting temperature in the lower mantle. Science 262, 553–555.

Zerr, A., Boehler, R., 1994. Constraints on the melting temperature of the lower mantle from high-pressure experiments on Mgo and magnesiowustite. Nature 371 (6497), 506–508.

Zerr, A., Diegeler, A., Boehler, R., 1998. Solidus of Earth's deep mantle. Science 281 (5374), 243–246.

Zhang, L., Fei, Y.W., 2008. Melting behavior of (Mg,Fe)O solid solutions at high pressure. Geophys. Res. Lett. 35, L13302.

Zhang, J.Z., Herzberg, C., 1994. Melting experiments on anhydrous peridotite KLB-1 from 5.0 to 22.5 GPa. J. Geophys. Res.-Solid Earth 99 (B9), 17729–17742.

Zhou, Y.H., Miller, G.H., 1997. Constraints from molecular dynamics on the liquidus and solidus of the lower mantle. Geochim. Cosmochim. Acta 61 (14), 2957–2976.